

Efficient Natural Gradient Descent Methods for Large-Scale Optimization Problems*

Levon Nurbekyan[†], Wanzhou Lei[‡], and Yunan Yang[§]

Abstract. We propose an efficient numerical method for computing natural gradient descent directions with respect to a generic metric in the state space. Our technique relies on representing the natural gradient direction as a solution to a standard least-squares problem. Hence, instead of calculating, storing, or inverting the information matrix directly, we apply efficient methods from numerical linear algebra to solve this least-squares problem. We treat both scenarios where the derivative of the state variable with respect to the parameter is either explicitly known or implicitly given through constraints. We apply the QR decomposition to solve the least-squares problem in the former case and utilize the adjoint-state method to compute the natural gradient descent direction in the latter case. As a result, we can reliably compute several natural gradient descents, including the Wasserstein natural gradient, for a large-scale parameter space with thousands of dimensions, which was believed to be out of reach. Finally, our numerical results shed light on the qualitative differences among the standard gradient descent method and various natural gradient descent methods based on different metric spaces in large-scale nonconvex optimization problems.

Key words. natural gradient, constrained optimization, least-squares method, gradient flow, inverse problem

AMS subject classifications. 65K10, 49M15, 49M41, 90C26, 49Q22

1. Introduction. Consider the following optimization problem

$$(1.1) \quad \inf_{\theta} f(\rho(\theta)),$$

where f is a loss function and $\rho(\theta)$ represents the state variable that depends on the parameter θ . A common approach to solve such a problem is via the gradient descent method whose continuous analog is the following gradient flow equation

$$\dot{\theta} = -\partial_{\theta} f(\rho(\theta)).$$

Although reasonably effective and computationally efficient, the gradient descent method might suffer from multiple local critical points in nonconvex problems and slow convergence due to a lack of information on the curvature. There have been numerous variations based on the stochastic gradient descent method [8] that utilize noises to escape local minima and saddle points. Other optimization algorithms have been developed to improve the speed of convergence, such as Newton's method, quasi-Newton methods [28], and various acceleration techniques [27] including momentum-based methods [32].

Among deterministic optimization methods that have provably faster convergence rates than the gradient descent method, a common idea is to incorporate the curvature information either directly or via momentum [32]. In this paper, we focus on one such method called the *natural gradient descent* [1, 2, 29, 23, 17, 18, 35, 22]. The method of natural gradient descent was initially proposed to solve optimization problems in the form of (1.1) for which the steepest descent is implemented with respect to the ρ -space (the state space where $\{\rho(\theta)\}$ live in) instead of the space

*Submitted to the editors on February 15, 2022.

Funding: L. Nurbekyan was partially supported by AFOSR MURI FA 9550 18-1-0502 grant. Y. Yang was partially supported by NSF grant DMS-1913129.

[†]Department of Mathematics, UCLA (lnurbek@math.ucla.edu).

[‡]New York University (w1860@nyu.edu).

[§]Institute for Theoretical Studies, ETH Zürich (yunan.yang@eth-its.ethz.ch).

of parameters (θ -space) [1, 2]. A Riemannian structure is imposed on the *parameterized* subset $\{\rho(\theta)\}$ and then pulled back into the θ -space, resulting in a natural gradient descent update in θ .

The underlying idea of the natural gradient descent method is to take advantage of the geometric structure and to find a direction with a maximum descent in the ρ -space. Based on the proximal operator, the ensuing iteration θ^{l+1} follows

$$(1.2) \quad \theta^{l+1} = \operatorname{argmin}_{\theta} \left\{ f(\rho(\theta)) + \frac{d_{\rho}(\rho(\theta), \rho(\theta^l))}{2\tau} \right\},$$

as opposed to finding a maximum descent in the θ -space as done by the “standard” gradient descent:

$$(1.3) \quad \theta^{l+1} = \operatorname{argmin}_{\theta} \left\{ f(\rho(\theta)) + \frac{d_{\theta}(\theta, \theta^l)}{2\tau} \right\},$$

where θ^l is the l -th iteration, τ is the step size, and d_{ρ} and d_{θ} are metrics for the ρ -space and θ -space, respectively. Intuitively, one may interpret that this is a shift from the parametric θ -space to the more “natural” ρ -space. Consequently, the infinitesimal decrease in the value of f and the direction of motion for ρ on \mathcal{M} at $\rho = \rho(\theta)$ are invariant under re-parameterizations [23].

Natural gradient descent has been proven to be advantageous in various problems in machine learning and statistical inference, such as blind source separation [3], reinforcement learning [30] and neural network training [25, 24, 23, 34, 29, 15, 35, 19]. Further applications include solution methods for high-dimensional Fokker–Planck equations [16, 21]. It is a natural framework to include the curvature of the loss function based on the natural Riemannian structure of the ρ -space [2], and thus accelerate the rate of convergence in the θ -space and directly control the model in the ρ -space instead of the θ -space. Unlike Newton’s method, the natural gradient method always preconditions the gradient with the inverse of a positive definite matrix [4]. It is also closely related to generalized Gauss–Newton methods [25, 34, 29] and many common optimization algorithms under the so-called Bayesian learning rule [14].

Despite its success in statistical inferences and machine learning [24, 36, 23, 29, 35, 19], the natural gradient descent method is far from being a mainstream computational technique. A major obstacle is its computational complexity. Mathematically, the natural gradient reduces to preconditioning the standard gradient by the inverse of the *information* or *curvature* matrix. The latter is dense and thus the numerical computation of its inverse is intractable. Therefore, existing work in the literature focused on explicit formulae [39], fast matrix-vector products [34, 25, 29, 23], and factorization techniques [24] for natural gradients generated by the Fisher–Rao metric in the ρ -space and $\{\rho(\theta)\}$ generated by feed-forward neural networks. Fast matrix-vector product methods exploit the “structural compatibility” of standard loss functions and the Fisher metric by interpreting the Fisher natural gradient descent as a generalized Gauss–Newton or Hessian-free optimization [23]. These methods take advantage of the computational aspects of feed-forward neural networks by recycling computations during the forward and backward passes through the network. Furthermore, computational methods for natural gradients generated by the Wasserstein metric in the ρ -space are either variational [15, 7, 19, 16, 21, 41] or relying on the entropic regularization of the Wasserstein distance [35]. The variational techniques are based on the proximal approximation (1.2), whereas entropic regularization techniques utilize computationally efficient Sinkhorn divergences [35].

This work aims to provide a unified computational framework and streamline the computation of a general natural gradient flow via the systematic application of efficient tools from numerical linear algebra. In particular, we allow for explicit and implicit models and do not rely on their specific structure, such as feed-forward neural networks. Moreover, our approach applies to a general metric for the state space, which can be independent of the choice of the loss function. As examples, we

treat Euclidean, Wasserstein, Sobolev, and Fisher–Rao natural gradients in a single framework for a general loss function. Besides, algorithms based on numerical linear algebra are generally more robust in performance and better understood in terms of analysis than their nonconvex variational counterparts. As a result, we can reliably compute the Wasserstein natural gradient for a parameter space of thousands of dimensions, which was believed to be out of reach [35].

The proposed approach takes advantage of the standard least-squares formulation of the natural gradient descent direction. In particular, when the derivative of the state variable with respect to the parameter, which we refer to as the tangent vector $\partial_\theta \rho$, is analytically available, we can utilize the (column-pivoting) QR decomposition of tangent vectors for which a low-rank approximation can be directly applied if necessary [13]. When $\partial_\theta \rho$ is not explicitly given but implicitly available through the optimization constraints, we take advantage of iterative solution procedures such as the conjugate gradient method [26] utilizing the adjoint-state method [31] for calculating the gradients. This second approach shares the same flavor with the method of fast matrix-vector product for the Fisher–Rao natural gradient descent for neural network training [34, 25, 29, 23]. As a result, we obtain efficient and robust numerical methods for natural gradient flows without directly calculating, storing, or inverting the dense information matrix. Using our proposed methods to compute the natural gradient, we perform numerical tests motivated by two computational inverse problems. In the first Gaussian mixture model, the tangent vector $\partial_\theta \rho$ is explicit, while the second example of full waveform inversion is a large-scale PDE-constrained optimization problem where $\partial_\theta \rho$ is too costly to compute. As mentioned above, our proposed unified analytical and numerical frameworks apply to general natural gradient methods. In particular, we concentrate on a few common natural gradients based on the Euclidean distance (L^2), the quadratic Wasserstein metric (W_2), the Sobolev norms (H^s and \dot{H}^s), and the Fisher–Rao metric. We remark that the L^2 natural gradient for the least-squares loss functions is precisely the Gauss–Newton method [28, 34, 29, 23].

The rest of the paper is organized as follows. In Section 2, we first present the general mathematical formulations of the natural gradient based on a given metric space (\mathcal{M}, g) and how it contrasts with the standard gradient. We then discuss a few common natural gradient examples and how they can all be reduced to a standard L^2 -based minimization problem on the continuous level. In Section 3, we demonstrate our general computational approaches under a unified framework that applies to any natural gradient descent method. The strategies concentrate on two scenarios regarding whether the tangent vector $\partial_\theta \rho$ is explicitly given or not, followed by Section 4 where we apply the proposed numerical strategies for natural gradient descent methods to optimization problems under these two scenarios. Conclusions and further discussions follow in Section 5.

2. Mathematical formulations of natural gradient descent. We begin by discussing the natural gradient descent method in an abstract setting before focusing on the common examples.

Assume that ρ is in a Riemannian manifold (\mathcal{M}, g) , and θ is in an open set $\Theta \subset \mathbb{R}^p$. Furthermore, assume that the correspondence $\theta \in \Theta \mapsto \rho(\theta) \in \mathcal{M}$ is smooth so that there exist tangent vectors

$$(2.1) \quad \left\{ \partial_{\theta_1}^g \rho(\theta), \partial_{\theta_2}^g \rho(\theta), \dots, \partial_{\theta_p}^g \rho(\theta) \right\} \subset T_\rho \mathcal{M}.$$

The superscript g in ∂^g highlights the dependence of tangent vectors on the choice of the Riemannian structure (\mathcal{M}, g) . Furthermore, assume that $f : \mathcal{M} \mapsto \mathbb{R}$ is a smooth function and denote by $\partial_\rho^g f \in T_\rho \mathcal{M}$ its metric gradient; that is, for all smooth curves $t \mapsto \rho(t)$, we have

$$\frac{df(\rho(t))}{dt} = \langle \partial_\rho^g f(\rho(t)), \partial_t^g \rho(t) \rangle_{g(\rho(t))}.$$

Tangent vectors $\{\partial_{\theta_i}^g \rho\}_{i=1}^p$ incorporate fundamental information on how $\rho(\theta)$ traverses \mathcal{M} when θ traverses Θ . Indeed, an infinitesimal motion of θ along coordinate θ_i axis in Θ induces an

infinitesimal motion of ρ along $\partial_{\theta_i}^g \rho$ in \mathcal{M} . More generally, if $\frac{d\theta}{dt} = \dot{\theta} = \eta = (\eta_1, \dots, \eta_p)^\top$, then

$$\partial_t^g \rho(\theta) = \eta_1 \partial_{\theta_1}^g \rho + \dots + \eta_p \partial_{\theta_p}^g \rho.$$

Consequently, we have that

$$\frac{df(\rho(\theta))}{dt} = \langle \partial_\rho^g f, \partial_t^g \rho(\theta) \rangle_{g(\rho(\theta))} = \langle \partial_\rho^g f, \sum_{i=1}^p \eta_i \partial_{\theta_i}^g \rho \rangle_{g(\rho(\theta))}.$$

Intuitively, in order to achieve the largest descent in the loss function $f(\rho(\theta))$, we want to choose $\eta = (\eta_1, \dots, \eta_p)^\top$ such that $\partial_\rho^g f$ is as *negatively* correlated with $\sum_{i=1}^p \eta_i \partial_{\theta_i}^g \rho$ as possible in term of the given metric g . Thus, the *natural gradient descent* direction corresponds to the best approximation of $-\partial_\rho^g f$ by $\{\partial_{\theta_i}^g \rho\}$ in $T_\rho \mathcal{M}$; that is,

$$(2.2) \quad \eta^{nat} = \underset{\eta}{\operatorname{argmin}} \left\| \partial_\rho^g f + \sum_{i=1}^p \eta_i \partial_{\theta_i}^g \rho \right\|_{g(\rho(\theta))}^2.$$

In other words, the natural gradient descent corresponds to the evolution of θ that attempts to follow the *manifold gradient descent of f on \mathcal{M}* as closely as possible.

A critical benefit of this choice is to help filter out the effects of a particular parameterization (since the corresponding decrease in the loss function is parameter-invariant) and reach $\operatorname{argmin}_{\rho \in \mathcal{M}} f(\rho)$ as quickly and as closely as possible. For the analysis of natural gradient descent based on this insight, we refer to [23, 21] for more details.

Remark 2.1. When $\{\partial_{\theta_i}^g \rho\}$ are linearly dependent, the η^{nat} in (2.2) is not unique, and we may pick the one with the minimal length.

To compare the natural gradient with the standard gradient $\partial_\theta f(\rho(\theta))$, first note that

$$\frac{df(\rho(\theta))}{dt} = \langle \partial_\rho^g f, \sum_{i=1}^p \eta_i \partial_{\theta_i}^g \rho \rangle_{g(\rho(\theta))} = \sum_{i=1}^p \langle \partial_\rho^g f, \partial_{\theta_i}^g \rho \rangle_{g(\rho(\theta))} \eta_i = \partial_\theta f(\rho(\theta)) \cdot \eta.$$

Therefore, in a similar form with (2.2), the standard gradient descent direction is the solution to

$$\eta^{std} = \underset{\eta}{\operatorname{argmin}} \|\partial_\theta f(\rho(\theta)) + \eta\|^2.$$

In other words, the standard gradient descent is the steepest direction in the θ -space, whereas the natural gradient descent is an approximation of the steepest descent direction in the ρ -space, in terms of a given metric g for the ρ -space.

Furthermore, (2.2) implies that under the natural gradient flow, the direction of motion for ρ on \mathcal{M} given by

$$(2.3) \quad \partial_t^g \rho = \sum_{i=1}^p \eta_i^{nat} \partial_{\theta_i}^g \rho$$

is the orthogonal projection of $-\partial_\rho^g f$ onto $\operatorname{span}\{\partial_{\theta_1}^g \rho, \dots, \partial_{\theta_p}^g \rho\}$. Since the latter is invariant under smooth changes of coordinates $\theta = \theta(\psi)$, we obtain that (2.3) is also invariant under such transformations. Additionally, the infinitesimal decay of the loss function is also invariant under smooth changes of the coordinates. Indeed,

$$\frac{df(\theta)}{dt} = -\|P \partial_\rho^g f\|_{g(\rho(\theta))}^2,$$

where $P\partial_\rho^g f$ denotes the orthogonal projection of $-\partial_\rho^g f$ onto $\text{span}\{\partial_{\theta_1}^g \rho, \dots, \partial_{\theta_p}^g \rho\}$ in $T_\rho \mathcal{M}$. These invariance properties mitigate potential negative effects of a poor choice of parameterization. In contrast, the standard gradient descent leads to

$$\begin{aligned}\partial_t^g \rho &= \sum_{i=1}^p \eta_i^{std} \partial_{\theta_i}^g \rho = - \sum_{i=1}^p \langle \partial_\rho^g f, \partial_{\theta_i}^g \rho \rangle_{g(\rho(\theta))} \partial_{\theta_i}^g \rho, \\ \frac{df(\theta)}{dt} &= - \|\partial_\theta f(\rho(\theta))\|_2^2 = - \sum_{i=1}^p \left| \langle \partial_\rho^g f, \partial_{\theta_i}^g \rho \rangle_{g(\rho(\theta))} \right|^2,\end{aligned}$$

which are not necessarily invariant under coordinate transformations.

When $\{\partial_{\theta_i}^g \rho\}$ are linearly independent, we obtain that

$$(2.4) \quad \eta^{nat} = -G(\theta)^{-1} \partial_\theta f(\rho(\theta)) = G(\theta)^{-1} \eta^{std},$$

where $G(\theta)$ is the *information matrix* whose (i, j) -th entry is

$$(2.5) \quad G_{ij}(\theta) = \langle \partial_{\theta_i}^g \rho, \partial_{\theta_j}^g \rho \rangle_{g(\rho(\theta))}, \quad i, j = 1, \dots, p.$$

Thus, we can regard a natural gradient descent direction as a standard gradient descent direction preconditioned by $G(\theta)^{-1}$, the inverse of the information matrix.

Since the information matrix $G(\theta)$ is often dense, direct application of (2.4) is prohibitively costly for high-dimensional parameter space; that is, large p . Our goal is to calculate η^{nat} via the least-squares formulation (2.2), circumventing the computational costs from assembling and inverting the dense matrix G directly.

2.1. L^2 natural gradient. In this subsection, we embed ρ in the metric space $(\mathcal{M}, g) = (L^2(\mathbb{R}^d), \langle \cdot, \cdot \rangle_{L^2(\mathbb{R}^d)})$. In this case, the tangent space $T_\rho \mathcal{M} = L^2(\mathbb{R}^d)$ for any $\rho \in \mathcal{M}$, and

$$\langle \zeta, \hat{\zeta} \rangle_{g(\rho)} = \int_{\mathbb{R}^d} \zeta(x) \hat{\zeta}(x) dx, \quad \forall \zeta, \hat{\zeta} \in T_\rho \mathcal{M}.$$

The linear structure of $L^2(\mathbb{R}^d)$ is advantageous for developing differential calculus, and many finite-dimensional concepts generalize naturally. Indeed, the tangent vectors (2.1) for a smooth mapping $\theta \in \Theta \mapsto \rho(\theta, \cdot) \in L^2(\mathbb{R}^d)$ are $\{\zeta_1, \zeta_2, \dots, \zeta_p\}$ given by

$$(2.6) \quad \zeta_i(x) = \partial_{\theta_i} \rho(\theta, x), \quad i = 1, \dots, p.$$

The information matrix in (2.5) is given by

$$G_{ij}^{L^2}(\theta) = \int_{\mathbb{R}^d} \partial_{\theta_i} \rho(\theta, x) \partial_{\theta_j} \rho(\theta, x) dx, \quad i, j = 1, 2, \dots, p.$$

Next, for $f : L^2(\mathbb{R}^d) \mapsto \mathbb{R}$, we obtain that the L^2 -derivative at ρ is $\partial_\rho f(\rho) \in L^2(\mathbb{R}^d)$ such that

$$(2.7) \quad \lim_{t \rightarrow 0} \frac{f(\rho + t\zeta) - f(\rho)}{t} = \int_{\mathbb{R}^d} \partial_\rho f(\rho)(x) \zeta(x) dx, \quad \forall \zeta \in L^2(\mathbb{R}^d).$$

Thus, $\partial_\rho f$ is the commonly known derivative in the sense of calculus of variations. Finally, for smooth $\rho : \Theta \rightarrow L^2(\mathbb{R}^d)$ and $f : L^2(\mathbb{R}^d) \rightarrow \mathbb{R}$, formula (2.2) leads to the L^2 natural gradient

$$(2.8) \quad \eta_{L^2}^{nat} = \underset{\eta \in \mathbb{R}^p}{\operatorname{argmin}} \left\| \partial_\rho f + \sum_{i=1}^p \eta_i \zeta_i \right\|_{L^2(\mathbb{R}^d)}^2.$$

2.2. H^s natural gradient. In this subsection, we assume that ρ is embedded in the L^2 -based Sobolev space $H^s(\mathbb{R}^d)$ for $s \in \mathbb{Z}$ (we return to the L^2 case if $s = 0$). The metric space $(\mathcal{M}, g) = (H^s(\mathbb{R}^d), \langle \cdot, \cdot \rangle_{H^s(\mathbb{R}^d)})$. Since this is also a Hilbert space, $T_\rho \mathcal{M} = H^s(\mathbb{R}^d)$ for all $\rho \in \mathcal{M}$, and

$$\langle \zeta, \hat{\zeta} \rangle_{g(\rho)} = \langle \zeta, \hat{\zeta} \rangle_{H^s(\mathbb{R}^d)} = \begin{cases} \int_{\mathbb{R}^d} \mathbf{D}^s \zeta \cdot \mathbf{D}^s \hat{\zeta} \, dx, & s \geq 0, \\ \int_{\mathbb{R}^d} \mathbf{D}^{-s} \chi \cdot \mathbf{D}^{-s} \hat{\chi} \, dx, & s < 0, \end{cases} \quad \zeta, \hat{\zeta} \in T_\rho \mathcal{M},$$

where \mathbf{D}^s is the linear operator whose output is the vector of all the partial derivatives up to order s for $s \geq 0$. For $s < 0$, we define $\chi = ((\mathbf{D}^{-s})^* \mathbf{D}^{-s})^{-1} \zeta$ and $\hat{\chi} = ((\mathbf{D}^{-s})^* \mathbf{D}^{-s})^{-1} \hat{\zeta}$. For example, $(\mathbf{D}^{-s})^* \mathbf{D}^{-s} = I - \Delta$ if $s = -1$ and $I - \Delta + \Delta^2$ if $s = -2$ [40]. Note that $\mathbf{D}^{-s}((\mathbf{D}^{-s})^* \mathbf{D}^{-s})^{-1} = ((\mathbf{D}^{-s})^*)^\dagger$ for $s < 0$, where † is the notation for pseudoinverse. Thus, we can rewrite

$$\langle \zeta, \hat{\zeta} \rangle_{H^s(\mathbb{R}^d)} = \langle \mathbf{D}^{-s} \chi, \mathbf{D}^{-s} \hat{\chi} \rangle_{L^2(\mathbb{R}^d)} = \langle ((\mathbf{D}^{-s})^*)^\dagger \zeta, ((\mathbf{D}^{-s})^*)^\dagger \hat{\zeta} \rangle_{L^2(\Omega)}, \quad \forall \zeta, \hat{\zeta} \in T_\rho \mathcal{M}.$$

For a smooth $\rho : \Theta \rightarrow H^s(\mathbb{R}^d)$, the tangent vectors are still $\{\zeta_i\}$ in (2.6) but now are considered as elements of $H^s(\mathbb{R}^d)$. This means that the information matrix $G^{H^s}(\theta)$ defined in (2.5) is given by

$$G_{ij}^{H^s}(\theta) = \langle \partial_{\theta_i} \rho, \partial_{\theta_j} \rho \rangle_{H^s(\mathbb{R}^d)} = \begin{cases} \int_{\mathbb{R}^d} \mathbf{D}^s \partial_{\theta_i} \rho(\theta, x) \cdot \mathbf{D}^s \partial_{\theta_j} \rho(\theta, x) \, dx, & s \geq 0, \\ \int_{\mathbb{R}^d} ((\mathbf{D}^{-s})^*)^\dagger \partial_{\theta_i} \rho(\theta, x) \cdot ((\mathbf{D}^{-s})^*)^\dagger \partial_{\theta_j} \rho(\theta, x) \, dx, & s < 0, \end{cases}$$

for $i, j = 1, \dots, p$. Note that G^{H^s} is different from G^{L^2} due to the inner product.

Next, we calculate the H^s gradient of smooth $f : H^s(\mathbb{R}^d) \rightarrow \mathbb{R}$. For $s \geq 0$, we have that

$$\lim_{t \rightarrow 0} \frac{f(\rho + t\zeta) - f(\rho)}{t} = \langle \partial_\rho^{H^s} f, \zeta \rangle_{H^s(\mathbb{R}^d)} = \int_{\mathbb{R}^d} \mathbf{D}^s \partial_\rho^{H^s} f \cdot \mathbf{D}^s \zeta \, dx = \int_{\mathbb{R}^d} (\mathbf{D}^s)^* \mathbf{D}^s \partial_\rho^{H^s} f \cdot \zeta \, dx,$$

and so from (2.7) we obtain

$$\partial_\rho^{H^s} f = ((\mathbf{D}^s)^* \mathbf{D}^s)^{-1} \partial_\rho f, \quad s \geq 0.$$

When $s < 0$, under analogue assumptions with the case $s \geq 0$, we have that

$$\begin{aligned} \lim_{t \rightarrow 0} \frac{f(\rho + t\zeta) - f(\rho)}{t} &= \langle \partial_\rho^{H^s} f, \zeta \rangle_{H^s(\mathbb{R}^d)} = \int_{\mathbb{R}^d} ((\mathbf{D}^{-s})^*)^\dagger \partial_\rho^{H^s} f \cdot ((\mathbf{D}^{-s})^*)^\dagger \zeta \, dx \\ &= \int_{\mathbb{R}^d} (\mathbf{D}^{-s})^\dagger ((\mathbf{D}^{-s})^*)^\dagger \partial_\rho^{H^s} f \cdot \zeta \, dx = \int_{\mathbb{R}^d} ((\mathbf{D}^{-s})^* \mathbf{D}^{-s})^\dagger \partial_\rho^{H^s} f \cdot \zeta \, dx. \end{aligned}$$

Thus, from (2.7), we have

$$\partial_\rho^{H^s} f = (\mathbf{D}^{-s})^* \mathbf{D}^{-s} \partial_\rho f, \quad s < 0.$$

Finally, for smooth $\rho : \Theta \rightarrow H^s(\mathbb{R}^d)$ and $f : H^s(\mathbb{R}^d) \rightarrow \mathbb{R}$, (2.2) leads to the H^s natural gradient

$$(2.9) \quad \eta_{H^s}^{nat} = \operatorname{argmin}_{\eta \in \mathbb{R}^p} \left\| \partial_\rho^{H^s} f + \sum_{i=1}^p \eta_i \zeta_i \right\|_{H^s(\mathbb{R}^d)}^2.$$

For numerical implementation, we reduce this previous formulation into a least-squares problem in $L^2(\mathbb{R}^d)$. More specifically, for $s \geq 0$, (2.9) can be written as

$$\eta_{H^s}^{nat} = \operatorname{argmin}_{\eta \in \mathbb{R}^p} \left\| \mathbf{D}^s ((\mathbf{D}^s)^* \mathbf{D}^s)^{-1} \partial_\rho f + \sum_{i=1}^p \eta_i \mathbf{D}^s \zeta_i \right\|_{L^2(\mathbb{R}^d)}^2.$$

Furthermore, for $s < 0$ we have that (2.9) can be written as

$$\eta_{H^s}^{nat} = \operatorname{argmin}_{\eta \in \mathbb{R}^p} \left\| \mathbf{D}^{-s} \partial_\rho f + \sum_{i=1}^p \eta_i ((\mathbf{D}^{-s})^*)^\dagger \zeta_i \right\|_{L^2(\mathbb{R}^d)}^2.$$

Both cases share the same form (2.10) with $\mathbf{L} = \mathbf{D}^s$ for $s \geq 0$ and $\mathbf{L} = ((\mathbf{D}^{-s})^*)^\dagger$ for $s < 0$:

$$(2.10) \quad \eta_{H^s}^{nat} = \operatorname{argmin}_{\eta \in \mathbb{R}^p} \left\| (\mathbf{L}^*)^\dagger \partial_\rho f + \sum_{i=1}^p \eta_i \mathbf{L} \zeta_i \right\|_{L^2(\mathbb{R}^d)}^2.$$

2.3. \dot{H}^s natural gradient. Next, we consider the natural gradient descent with respect to the Sobolev semi-norm \dot{H}^s . For simplicity, we assume that ρ is supported in a smooth bounded domain $\Omega \subset \mathbb{R}^d$. For $s > 0$, we define the space $\dot{H}^s(\Omega) = \{\zeta \in H^s(\Omega) : \int_\Omega \zeta = 0\}$ with the inner product

$$\langle \zeta, \hat{\zeta} \rangle_{\dot{H}^s(\Omega)} = \langle \tilde{\mathbf{D}}^s \zeta, \tilde{\mathbf{D}}^s \hat{\zeta} \rangle_{L^2(\Omega)} = \int_\Omega \tilde{\mathbf{D}}^s \zeta \cdot \tilde{\mathbf{D}}^s \hat{\zeta} dx, \quad \forall \zeta, \hat{\zeta} \in \dot{H}^s(\Omega),$$

where $\tilde{\mathbf{D}}^s$ is the linear operator whose output is the vector of all partial derivatives of positive order up to s . To consider the \dot{H}^s natural gradient flows, we embed ρ in (\mathcal{M}, g) , where

$$\mathcal{M} = \left\{ \rho \in H^s(\Omega) : \int_\Omega \rho = 1 \right\}, \quad T_\rho \mathcal{M} = \dot{H}^s(\Omega), \quad \langle \zeta, \hat{\zeta} \rangle_{g(\rho)} = \langle \zeta, \hat{\zeta} \rangle_{\dot{H}^s(\Omega)}, \quad \forall \zeta, \hat{\zeta} \in T_\rho \mathcal{M}.$$

For a smooth $\rho : \Theta \rightarrow \mathcal{M}$, we still have that the tangent vectors are $\{\zeta_i\}$ as defined in (2.6). Since $\int_\Omega \rho(\theta, x) dx = 1$ for all $\theta \in \Theta$, we have that

$$\int_\Omega \zeta_i(x) dx = \int_\Omega \partial_{\theta_i} \rho(\theta, x) dx = \partial_{\theta_i} \int_\Omega \rho(\theta, x) dx = 0, \quad i = 1, \dots, p,$$

and thus $\{\zeta_i\} \subset T_\rho \mathcal{M}$. The information matrix (2.5) for this case is $G^{\dot{H}^s}(\theta)$ given by

$$G_{ij}^{\dot{H}^s}(\theta) = \langle \partial_{\theta_i} \rho, \partial_{\theta_j} \rho \rangle_{\dot{H}^s(\Omega)} = \int_\Omega \tilde{\mathbf{D}}^s \partial_{\theta_i} \rho(\theta, x) \cdot \tilde{\mathbf{D}}^s \partial_{\theta_j} \rho(\theta, x) dx, \quad i, j = 1, \dots, p.$$

On the other hand, for $f : \mathcal{M} \rightarrow \mathbb{R}$, we have that $\partial_\rho^{\dot{H}^s} f \in \dot{H}^s(\Omega)$ where $\forall \zeta \in T_\rho \mathcal{M}$,

$$\lim_{t \rightarrow 0} \frac{f(\rho + t\zeta) - f(\rho)}{t} = \langle \partial_\rho^{\dot{H}^s} f, \zeta \rangle_{\dot{H}^s(\Omega)} = \int_\Omega \tilde{\mathbf{D}}^s \partial_\rho^{\dot{H}^s} f \cdot \tilde{\mathbf{D}}^s \zeta dx = \int_\Omega (\tilde{\mathbf{D}}^s)^* \tilde{\mathbf{D}}^s \partial_\rho^{\dot{H}^s} f \cdot \zeta dx.$$

The adjoint $(\tilde{\mathbf{D}}^s)^*$ is taken with respect to the $L^2(\Omega)$ inner product. Hence, based on (2.7),

$$(2.11) \quad \int_\Omega \left(\partial_\rho f - (\tilde{\mathbf{D}}^s)^* \tilde{\mathbf{D}}^s \partial_\rho^{\dot{H}^s} f \right) \cdot \zeta dx = 0, \quad \forall \zeta \in T_\rho \mathcal{M}.$$

Furthermore, denote by $\mathbf{1}$ the constant function that is equal to 1 on Ω . We then have that

$$T_\rho \mathcal{M} = \operatorname{span}\{\mathbf{1}\}^\perp = \ker(\tilde{\mathbf{D}}^s)^\perp = \operatorname{Im}((\tilde{\mathbf{D}}^s)^*),$$

where $^\perp$ is again taken with respect to the $L^2(\Omega)$ inner product. Hence, using the properties of adjoint operators, we obtain

$$\partial_\rho^{\dot{H}^s} f = \left((\tilde{\mathbf{D}}^s)^* \tilde{\mathbf{D}}^s \right)^\dagger \partial_\rho f, \quad s > 0.$$

Next, we discuss the case $s < 0$. As the dual space of $\dot{H}^{-s}(\Omega)$, the space $\dot{H}^s(\Omega)$ is equipped with the dual norm

$$\|\zeta\|_{\dot{H}^s(\Omega)} = \sup \left\{ \langle \zeta, \phi \rangle : \|\phi\|_{\dot{H}^{-s}(\Omega)} \leq 1 \right\}.$$

Using the Poincaré inequality and the Riesz representation theorem, we obtain that for every $\zeta \in \text{span}\{\mathbf{1}\}^\perp$, the map $\phi \mapsto \int_\Omega \zeta \phi$ is a continuous linear operator on $\dot{H}^{-s}(\Omega)$, and there exists a unique $\chi \in \dot{H}^{-s}(\Omega)$ such that

$$\int_\Omega \zeta \phi \, dx = \int_\Omega \tilde{\mathbf{D}}^{-s} \chi \, \tilde{\mathbf{D}}^{-s} \phi \, dx, \quad \forall \phi \in \dot{H}^{-s}(\Omega).$$

Hence, $\zeta = (\tilde{\mathbf{D}}^{-s})^* \tilde{\mathbf{D}}^{-s} \chi$ together with the homogeneous Neumann boundary condition. Therefore,

$$\|\zeta\|_{\dot{H}^s(\Omega)} = \|\tilde{\mathbf{D}}^{-s} \chi\|_{L^2} = \|\chi\|_{\dot{H}^{-s}(\Omega)}.$$

Using similar arguments for the $s > 0$ case, we obtain that

$$\langle \zeta, \hat{\zeta} \rangle_{\dot{H}^s(\Omega)} = \langle \tilde{\mathbf{D}}^{-s} \chi, \tilde{\mathbf{D}}^{-s} \hat{\chi} \rangle_{L^2(\Omega)} = \left\langle ((\tilde{\mathbf{D}}^{-s})^*)^\dagger \zeta, ((\tilde{\mathbf{D}}^{-s})^*)^\dagger \hat{\zeta} \right\rangle_{L^2(\Omega)}, \quad \forall \zeta, \hat{\zeta} \in \text{span}\{\mathbf{1}\}^\perp.$$

For more details on $\dot{H}^s(\Omega)$ where $s < 0$, we refer to [5, Lecture 13].

Next, we embed ρ in space $\mathcal{M} = \{\rho \in L^2(\Omega) : \int_\Omega \rho = 1\}$ with $T_\rho \mathcal{M} = \text{span}\{\mathbf{1}\}^\perp$ and

$$\langle \zeta, \hat{\zeta} \rangle_{g(\rho)} = \left\langle ((\tilde{\mathbf{D}}^{-s})^*)^\dagger \zeta, ((\tilde{\mathbf{D}}^{-s})^*)^\dagger \hat{\zeta} \right\rangle_{L^2(\Omega)}, \quad \forall \zeta, \hat{\zeta} \in T_\rho \mathcal{M}.$$

Furthermore, for a smooth function $f : \mathcal{M} \rightarrow \mathbb{R}$, we have that

$$\lim_{t \rightarrow 0} \frac{f(\rho + t\zeta) - f(\rho)}{t} = \langle \partial_\rho^{\dot{H}^s} f, \zeta \rangle_{\dot{H}^s(\Omega)} = \int_\Omega ((\tilde{\mathbf{D}}^{-s})^* \tilde{\mathbf{D}}^{-s})^\dagger \partial_\rho^{\dot{H}^s} f \, \zeta \, dx.$$

Together with (2.7), we have

$$\int_\Omega \left(\partial_\rho f - ((\tilde{\mathbf{D}}^{-s})^* \tilde{\mathbf{D}}^{-s})^\dagger \partial_\rho^{\dot{H}^s} f \right) \zeta \, dx = 0, \quad \forall \zeta \in T_\rho \mathcal{M}.$$

After performing analysis similar to the $s > 0$ case, we obtain that

$$\partial_\rho^{\dot{H}^s} f = (\tilde{\mathbf{D}}^{-s})^* \tilde{\mathbf{D}}^{-s} \partial_\rho f, \quad s < 0.$$

Finally, for both $s > 0$ and $s < 0$ cases, (2.2) leads to the \dot{H}^s natural gradient

$$(2.12) \quad \eta_{\dot{H}^s}^{\text{nat}} = \underset{\eta \in \mathbb{R}^p}{\operatorname{argmin}} \left\| \partial_\rho^{\dot{H}^s} f + \sum_{i=1}^p \eta_i \zeta_i \right\|_{\dot{H}^s(\mathbb{R}^d)}^2,$$

for smooth $\rho : \Theta \rightarrow \mathcal{M}$ and $f : \mathcal{M} \rightarrow \mathbb{R}$. As before, we can rewrite (2.12) as a least-squares problem

$$(2.13) \quad \eta_{\dot{H}^s}^{\text{nat}} = \underset{\eta \in \mathbb{R}^p}{\operatorname{argmin}} \left\| (\mathbf{L}^*)^\dagger \partial_\rho f + \sum_{i=1}^p \eta_i \mathbf{L} \zeta_i \right\|_{L^2(\Omega)}^2, \quad \mathbf{L} = \begin{cases} \tilde{\mathbf{D}}^s, & s > 0 \\ ((\tilde{\mathbf{D}}^{-s})^*)^\dagger, & s < 0 \end{cases}.$$

Note that (2.13) shares the same form with (2.10).

2.4. Fisher–Rao–Hellinger natural gradient. Here, we assume that ρ is a strictly positive probability density function. We embed ρ in $(\mathcal{M}, g) = (L^1(\mathbb{R}^d), g)$ where $T_\rho(\mathcal{M}) = L^2_{\rho^{-1}}(\mathbb{R}^d)$ and

$$\langle \zeta, \hat{\zeta} \rangle_{g(\rho)} = \int_{\mathbb{R}^d} \frac{\zeta(x) \hat{\zeta}(x)}{\rho(x)} dx, \quad \forall \zeta, \hat{\zeta} \in T_\rho \mathcal{M}.$$

This Riemannian metric is called the Fisher–Rao metric, and the distance induced by this metric is the Hellinger distance: $d_H(\rho_1, \rho_2) \propto \|\sqrt{\rho_1} - \sqrt{\rho_2}\|_{L^2(\mathbb{R}^d)}$.

For a smooth $\rho : \Theta \rightarrow \mathcal{M}$, we have that the tangent vectors are $\{\zeta_i\}$ in (2.6) but now considered as elements of $L^2_{\rho^{-1}}(\mathbb{R}^d)$. Therefore, the information matrix in (2.5) becomes $G^{FR}(\theta) \in \mathbb{R}^{p \times p}$ where

$$G_{ij}^{FR}(\theta) = \int_{\mathbb{R}^d} \frac{\partial_{\theta_i} \rho(\theta, x) \partial_{\theta_j} \rho(\theta, x)}{\rho(\theta, x)} dx, \quad i, j = 1, 2, \dots, p.$$

As before, $G^{FR}(\theta)$ is in general different from $G^{L^2}(\theta)$, $G^{H^s}(\theta)$ and $G^{\dot{H}^s}(\theta)$.

Furthermore, for a smooth function $f : \mathcal{M} \rightarrow \mathbb{R}$, we have that

$$\lim_{t \rightarrow 0} \frac{f(\rho + t\zeta) - f(\rho)}{t} = \int_{\mathbb{R}^d} \frac{\partial_\rho^{FR} f}{\rho} \zeta dx,$$

and so from (2.7) we obtain

$$\partial_\rho^{FR} f = \rho \partial_\rho f.$$

Finally, for smooth $\rho : \Theta \rightarrow \mathcal{M}$ and $f : \mathcal{M} \rightarrow \mathbb{R}$, (2.2) leads to the Fisher–Rao natural gradient

$$(2.14) \quad \eta_{FR}^{nat} = \operatorname{argmin}_{\eta \in \mathbb{R}^p} \left\| \partial_\rho^{FR} f + \sum_{i=1}^p \eta_i \zeta_i \right\|_{L^2_{\rho^{-1}}(\mathbb{R}^d)}^2.$$

The L^2 least-squares formulation is

$$(2.15) \quad \eta_{FR}^{nat} = \operatorname{argmin}_{\eta \in \mathbb{R}^p} \left\| \frac{\partial_\rho^{FR} f}{\sqrt{\rho}} + \sum_{i=1}^p \eta_i \frac{\zeta_i}{\sqrt{\rho}} \right\|_{L^2(\mathbb{R}^d)}^2 = \operatorname{argmin}_{\eta \in \mathbb{R}^p} \left\| (\mathbf{L}^*)^\dagger \partial_\rho f + \sum_{i=1}^p \eta_i \mathbf{L} \zeta_i \right\|_{L^2(\mathbb{R}^d)}^2,$$

where $\mathbf{L}\zeta = \frac{1}{\sqrt{\rho}}\zeta$ and $(\mathbf{L}^*)^\dagger \partial_\rho f = \sqrt{\rho} \partial_\rho f$.

2.5. W_2 natural gradient. Denoting by $\mathcal{P}(\mathbb{R}^d)$ the set of Borel probability measures on \mathbb{R}^d , we first introduce the Wasserstein metric on the space $\mathcal{P}(\mathbb{R}^d)$. Furthermore, for $\rho \in \mathcal{P}(\mathbb{R}^d)$ and a measurable function $f : \mathbb{R}^d \rightarrow \mathbb{R}^n$, we denote by $f_\# \rho \in \mathcal{P}(\mathbb{R}^n)$ the probability measure defined by

$$(f_\# \rho)(B) = \rho(f^{-1}(B)), \quad \forall B \subset \mathbb{R}^n \text{ Borel},$$

and call it the pushforward of ρ under f . Next, for any $\rho_1, \rho_2 \in \mathcal{P}(\mathbb{R}^d)$, we denote $\Gamma(\rho_1, \rho_2)$ as the set of all possible joint measure $\pi \in \mathcal{P}(\mathbb{R}^{2d})$ such that

$$\int_{\mathbb{R}^{2d}} (\phi(x) + \psi(y)) d\pi(x, y) = \int_{\mathbb{R}^d} \phi(x) d\rho_1(x) + \int_{\mathbb{R}^d} \psi(y) d\rho_2(y)$$

for all $(\phi, \psi) \in L^1(\rho_1) \times L^1(\rho_2)$. The 2-Wasserstein distance is defined as

$$W_2(\rho_1, \rho_2) = \left(\inf_{\pi \in \Gamma(\rho_1, \rho_2)} \int_{\mathbb{R}^{2d}} |x - y|^2 d\pi(x, y) \right)^{\frac{1}{2}}.$$

Denoting by $\mathcal{P}_2(\mathbb{R}^d)$ the set of Borel probability measures with finite second moments, we have that $(\mathcal{P}_2(\mathbb{R}^d), W_2)$ is a complete separable metric space; see more details in [37, Chapters 7] and [6, Chapters 7]. More intriguingly, one can build a Riemannian structure on $(\mathcal{P}_2(\mathbb{R}^d), W_2)$. Our discussion is formal and we refer to [37, Chapters 8] and [6, Chapters 8] for rigorous treatments.

In short, tangent vectors in $(\mathcal{P}_2(\mathbb{R}^d), W_2)$ are the infinitesimal spatial displacements of minimal kinetic energy. More specifically, for a given $\rho \in \mathcal{P}_2(\mathbb{R}^d)$, we define the tangent space, $T_\rho \mathcal{P}_2(\mathbb{R}^d)$, as a set of all maps $v \in L^2_\rho(\mathbb{R}^d; \mathbb{R}^d)$ such that

$$(2.16) \quad \|v + w\|_{L^2_\rho(\mathbb{R}^d; \mathbb{R}^d)} \geq \|v\|_{L^2_\rho(\mathbb{R}^d; \mathbb{R}^d)}, \quad \forall w \in L^2_\rho(\mathbb{R}^d; \mathbb{R}^d) \quad \text{s.t.} \quad \nabla \cdot (w\rho) = 0,$$

where $L^2_\rho(\mathbb{R}^d; \mathbb{R}^d)$ denotes the ρ -weighted L^2 space. When $\rho = 1$, it reduces to the standard L^2 . The divergence equation above is understood in the sense of distributions; that is,

$$\int_{\mathbb{R}^d} \nabla \phi(x) \cdot w(x) \rho(x) dx = 0, \quad \forall \phi \in C_c^\infty(\mathbb{R}^d).$$

If we think of ρ as a fluid density, then an infinitesimal displacement $\frac{dx}{dt} = \dot{x} = v(x)$ leads to an infinitesimal density change given by the continuity equation

$$(2.17) \quad \frac{\partial \rho}{\partial t} = -\nabla \cdot (v\rho).$$

Therefore, for a given w such that $\nabla \cdot (w\rho) = 0$, we have that both $\dot{x} = v(x)$ and $\dot{x} = v(x) + w(x)$ lead to the same continuity equation (2.17). Therefore, the evolution of the density is insensitive to the divergence-free vector fields, and we project them out leaving only a unique vector field with the minimal kinetic energy. The kinetic energy of a vector field v is then defined as

$$\|v\|_{L^2_\rho(\mathbb{R}^d; \mathbb{R}^d)}^2 = \int_{\mathbb{R}^d} |v(x)|^2 \rho(x) dx.$$

For a given evolution $t \mapsto \rho(t, \cdot)$, such a “distilled” vector field v is unique and incorporates critical geometric information on the spatial evolution of ρ .

Next, we define a Riemannian metric by

$$\langle v, \hat{v} \rangle_{g(\rho)} = \int_{\mathbb{R}^d} v(x) \cdot \hat{v}(x) \rho(x) dx, \quad v, \hat{v} \in T_\rho \mathcal{P}_2(\mathbb{R}^d).$$

Furthermore, a mapping $\theta \in \Theta \mapsto \rho(\theta, \cdot) \in \mathcal{P}(\mathbb{R}^d)$ is differentiable if for every $\theta \in \Theta$, there exists a set of bases $\{v_i(\theta)\} \subset T_\rho \mathcal{P}_2(\mathbb{R}^d)$ such that

$$(2.18) \quad \lim_{t \rightarrow 0} \frac{W_2(\rho(\theta + t\eta), (I + t \sum_{i=1}^p \eta_i v_i(\theta)) \# \rho(\theta))}{t} = 0, \quad \forall \eta \in \mathbb{R}^p,$$

where I is the identity map. Thus,

$$(2.19) \quad \{v_1, v_2, \dots, v_p\} = \{\partial_{\theta_1}^W \rho, \partial_{\theta_2}^W \rho, \dots, \partial_{\theta_p}^W \rho\},$$

are the tangent vectors in (2.1) for the W_2 metric.

For $f : \mathcal{P}_2(\mathbb{R}^d) \rightarrow \mathbb{R}$, the Wasserstein gradient at ρ is then $\partial_\rho^W f(\rho) \in T_\rho \mathcal{P}_2(\mathbb{R}^d)$, such that

$$(2.20) \quad \lim_{t \rightarrow 0} \frac{f((I + tv) \# \rho) - f(\rho)}{t} = \int_{\mathbb{R}^d} \partial_\rho^W f(\rho)(x) \cdot v(x) \rho(x) dx, \quad \forall v \in T_\rho \mathcal{P}(\mathbb{R}^d).$$

Thus, for a smooth $\rho : \Theta \rightarrow \mathcal{P}_2(\mathbb{R}^d)$ and $f : \mathcal{P}_2(\mathbb{R}^d) \rightarrow \mathbb{R}$, we have the W_2 natural gradient descent direction for θ given by

$$(2.21) \quad \eta_{W_2}^{nat} = \operatorname{argmin}_{\eta \in \mathbb{R}^p} \left\| \partial_\rho^W f + \sum_{i=1}^p \eta_i v_i \right\|_{L_\rho^2(\mathbb{R}^d; \mathbb{R}^d)}^2.$$

As seen in (2.6), the L^2 derivatives and gradients are typically easier to calculate. Here, we discuss the relations between the L^2 and W_2 metrics that are useful for calculating the W_2 derivatives and gradients, i.e., $\{v_i\}$ and $\partial_\rho^W f$. We formulate the main conclusions in [Proposition 2.2](#).

Proposition 2.2. *Let $\{\zeta_i\}$ and $\{v_i\}$ follow (2.6) and (2.19), respectively. The $\partial_\rho f$ and $\{\zeta_i\}$ in (2.8) relate to the $\partial_\rho^W f$ and $\{v_i\}$ in (2.21) as follows.*

$$(2.22) \quad \partial_\rho^W f = \nabla \partial_\rho f,$$

$$(2.23) \quad v_i(\theta) = \operatorname{argmin}_v \left\{ \|v\|_{L_{\rho(\theta)}^2(\mathbb{R}^d; \mathbb{R}^d)}^2 : -\nabla \cdot (\rho(\theta)v) = \zeta_i(\theta) \right\}, \quad i = 1, \dots, p.$$

Informal derivation. Given a vector field v and a small $t > 0$, we have that $I + tv$ is a first-order approximation of the trajectory below where I is the identity function. Note that in Lagrangian coordinates, $\dot{x} = v(x)$. Thus, from the continuity equation (2.17), we have that

$$(2.24) \quad (I + tv) \# \rho = \rho - t \nabla \cdot (\rho v) + o(t).$$

Recall that $\zeta_i = \partial_{\theta_i} \rho$ and $v_i = \partial_{\theta_i}^W \rho$. Using this observation together with (2.6) and (2.18), we have

$$\begin{aligned} \rho(\theta + t\eta) &= \rho(\theta) + t \sum_{i=1}^p \eta_i \zeta_i(\theta) + o(t), \\ \rho(\theta + t\eta) &= \rho(\theta) - t \sum_{i=1}^p \eta_i \nabla \cdot (\rho(\theta) v_i(\theta)) + o(t), \end{aligned}$$

for all $\eta \in \mathbb{R}^p$. By comparing the above two equations, we have

$$(2.25) \quad -\nabla \cdot (\rho(\theta) v_i(\theta)) = \zeta_i(\theta), \quad 1 \leq i \leq p.$$

After taking (2.16) into account, we obtain (2.23).

Next, we establish a connection between $\partial_\rho f$ and $\partial_\rho^W f$. Combining (2.7), (2.20), (2.24)-(2.25),

$$\int_{\mathbb{R}^d} \partial_\rho^W f(\rho)(x) \cdot v(x) \rho(x) dx = - \int_{\mathbb{R}^d} \partial_\rho f(\rho)(x) \nabla \cdot (\rho(x) v(x)) dx = \int_{\mathbb{R}^d} \nabla \partial_\rho f(\rho)(x) \cdot v(x) \rho(x) dx,$$

for all $v \in T_\rho \mathcal{P}_2(\mathbb{R}^d)$. Hence, we obtain (2.22). ■

Similar to previous cases, we want to turn (2.21) into an unweighted L^2 formulation. Using results in [Proposition 2.2](#), we know that the Wasserstein tangent vectors at ρ are velocity fields of minimal kinetic energy in $L_\rho^2(\mathbb{R}^d; \mathbb{R}^d)$. We first perform a change of variables

$$\tilde{v}_i = \sqrt{\rho} v_i, \quad i = 1, \dots, p,$$

where the set of $\{v_i\}$ follows (2.19). As a result, for each $i = 1, \dots, p$, (2.23) reduces to

$$(2.26) \quad \tilde{v}_i(\theta) = \operatorname{argmin} \left\{ \|\tilde{v}\|_{L^2(\mathbb{R}^d; \mathbb{R}^d)}^2 : \mathbf{B} \tilde{v} = \zeta_i(\theta) \right\}, \quad \text{where } \mathbf{B} \tilde{v} = -\nabla \cdot (\sqrt{\rho(\theta)} \tilde{v}).$$

We then have $\tilde{v}_i = \mathbf{B}^\dagger \zeta_i$ for $i = 1, \dots, p$. Denote the adjoint operator of \mathbf{B} as \mathbf{B}^* . Note that $\mathbf{B}^* \eta = \sqrt{\rho} \nabla \eta$. Combining these observations with [Proposition 2.2](#), formulation (2.21) becomes

$$(2.27) \quad \begin{aligned} \eta_{W_2}^{nat} &= \operatorname{argmin}_{\eta \in \mathbb{R}^p} \left\| \sqrt{\rho} \nabla \partial_\rho f + \sum_{i=1}^p \eta_i \tilde{v}_i \right\|_{L^2(\mathbb{R}^d; \mathbb{R}^d)}^2 = \operatorname{argmin}_{\eta \in \mathbb{R}^p} \left\| \mathbf{B}^* \partial_\rho f + \sum_{i=1}^p \eta_i \mathbf{B}^\dagger \zeta_i \right\|_{L^2(\mathbb{R}^d; \mathbb{R}^d)}^2 \\ &= \operatorname{argmin}_{\eta \in \mathbb{R}^p} \left\| (\mathbf{L}^*)^\dagger \partial_\rho f + \sum_{i=1}^p \eta_i \mathbf{L} \zeta_i \right\|_{L^2(\mathbb{R}^d; \mathbb{R}^d)}^2, \quad \text{where } \mathbf{L} = \mathbf{B}^\dagger. \end{aligned}$$

We have reformulated the W_2 natural gradient descent as a standard L^2 minimization (2.27).

Remark 2.3. Note that Wasserstein natural gradient is closely related to the \dot{H}^{-1} natural gradient presented in [Subsection 2.3](#). Indeed, taking $s = -1$ in (2.13) we obtain that

$$\eta_{\dot{H}^{-1}}^{nat} = \operatorname{argmin}_{\eta \in \mathbb{R}^p} \left\| \nabla \partial_\rho f + \sum_{i=1}^p \eta_i (\nabla^*)^\dagger \zeta_i \right\|_{L^2(\Omega)}^2,$$

which matches (2.27) except that the weighted divergence operator \mathbf{B} defined in (2.26) is replaced with the unweighted divergence operator $-\nabla \cdot = \nabla^*$. When $\rho(\theta) \equiv 1$, these two operators coincide.

In principle, one may consider natural gradient descents generated by the generalized operator

$$\mathbf{B}_k \tilde{v} = -\nabla \cdot (\rho(\theta)^k \tilde{v}), \quad \mathbf{L} = (\mathbf{B}_k)^\dagger,$$

where the case $k = 0$ corresponds to the \dot{H}^{-1} natural gradient and $k = 1/2$ corresponds to the W_2 natural gradient descent. The term ρ^k is often referred to as mobility in gradient flow equations [20].

Remark 2.4. Natural gradient descents based upon the L^2 norm (2.8), the H^s norm (2.9), the \dot{H}^s norm (2.12), the Fisher–Rao metric (2.14) and the W_2 metric (2.21) are similar in form but equipped with different underlying metric space (\mathcal{M}, g) for ρ . All of them can be reduced to the same common form but with a different \mathbf{L} operator; see (2.8), (2.10), (2.13), (2.15) and (2.27), respectively. As a result, we expect that they may perform differently in the optimization process as natural gradient descent methods, which we will see later from numerical examples in [Section 4](#).

2.6. Gauss–Newton algorithm as an L^2 natural gradient. Assume that f measures the least-squares difference between the model $\rho(x; \theta)$ and the reference $\rho^*(x)$ distributions; that is,

$$(2.28) \quad f(\rho(\theta)) = \frac{1}{2} \int_{\Omega} |\rho(x; \theta) - \rho^*(x)|^2 dx,$$

where Ω is the spatial domain. Thus, the problem of finding the parameter θ becomes

$$\inf_{\theta} f(\rho(\theta)) = \inf_{\theta} \frac{1}{2} \int_{\Omega} |\rho(x; \theta) - \rho^*(x)|^2 dx = \inf_{\theta} \frac{1}{2} \int_{\Omega} |r(x; \theta)|^2 dx, \quad r(x; \theta) = \rho(x; \theta) - \rho^*(x).$$

We will denote $\rho(x; \theta)$ as $\rho(\theta)$ and $r(x; \theta)$ as $r(\theta)$.

The Gauss–Newton (GN) algorithm [28] is one popular computational method to solve this nonlinear least-squares problem. In the continuous limit, the algorithm reduces to the flow

$$(2.29) \quad \dot{\theta} = \eta^{GN} = \operatorname{argmin}_{\eta \in \mathbb{R}^p} \left\| r(\theta) + \sum_{i=1}^p \partial_{\theta_i} r(\theta) \eta_i \right\|_{L^2(\Omega)}^2 = \operatorname{argmin}_{\eta \in \mathbb{R}^p} \left\| \rho(\theta) - \rho^* + \sum_{i=1}^p \partial_{\theta_i} \rho(\theta) \eta_i \right\|_{L^2(\Omega)}^2$$

where we choose a minimal-norm η if there are multiple solutions. The algorithm is based on a first-order approximation of the residual term $r(\theta + \eta) = r(\theta) + \sum_{i=1}^p \partial_{\theta_i} r(\theta) \eta_i + o(\eta)$.

A key observation is that (2.29) is precisely the L^2 natural gradient flow. Indeed, we have that

$$\lim_{t \rightarrow 0} \frac{f(\rho + t\zeta) - f(\rho)}{t} = \int_{\Omega} (\rho(\theta) - \rho^*) \zeta(x) dx,$$

and therefore $\partial_{\rho} f(\rho) = \rho(\theta) - \rho^*$. As a result, (2.8) reduces to (2.29) precisely.

The convergence rate of the GN method is between linear and quadratic based on various conditions [28]. Typically, the method is viewed as an alternative to Newton's method if one aims for faster convergence than gradient descent but does not want to compute/store the whole Hessian.

Remark 2.5. The L^2 natural gradient flow perspective of interpreting the GN algorithm suggests that mature numerical techniques for the GN algorithm are also applicable to *general* natural gradient descent methods, including those we introduced earlier in Section 2. For further connections between GN algorithms, Hessian-free optimization and natural gradient descent see discussions and references in [34, 29, 24, 23].

3. General computational approach. In this section, we discuss our general strategy to calculate the natural gradient descent directions. As mentioned earlier, our approach is based on efficient least-squares solvers since the problem of finding the natural gradient descent direction can be formulated as (2.2). In particular, we will introduce strategies when the tangent vector $\partial_{\theta} \rho$ cannot be obtained explicitly, which is the case for large-scale PDE-constrained optimization problems. We will first describe the general strategies and then explain how to apply these techniques to different types of natural gradient discussed in Section 2. We will work in the discrete setting hereafter.

By slightly abusing the notation, we assume that $\rho : \Theta \rightarrow \mathbb{R}^k$ is a proper discretization of $\theta \mapsto \rho(\theta)$ while $\Theta \subseteq \mathbb{R}^p$. Similarly, let $f : \mathbb{R}^k \rightarrow \mathbb{R}$ be a suitable discretization of $\rho \mapsto f(\rho)$. Hence, the standard finite-dimensional gradient and Jacobian, $\partial_{\rho} f \in \mathbb{R}^k$ and $\partial_{\theta} \rho \in \mathbb{R}^{k \times p}$, are discretizations of their continuous counterparts discussed in Subsection 2.1. In particular, we denote the Jacobian

$$(3.1) \quad Z = (\zeta_1 \ \zeta_2 \ \cdots \ \zeta_p) = \partial_{\theta} \rho, \quad \text{where } \zeta_j = \partial_{\theta_j} \rho.$$

Without loss of generality, we always assume $k > p$. That is, we have more data than parameters.

3.1. A unified framework. For numerical computation, our main proposal is to translate the general formula (2.2) and (2.4) for the natural gradient descent direction into a discrete least-squares formulation, given any Riemannian metric space (\mathcal{M}, g) .

Based on (2.8), the discrete L^2 natural gradient problem reduces to the least-squares problem

$$\eta^{nat} = \operatorname{argmin}_{\eta \in \mathbb{R}^p} \|\partial_{\rho} f + Z\eta\|_2^2.$$

As we have seen in Section 2, besides L^2 , the computation of the H^s , \dot{H}^s , Fisher–Rao, and Wasserstein natural gradient descent directions can also be formulated as a least-squares problem

$$(3.2) \quad \eta_L^{nat} = \operatorname{argmin}_{\eta \in \mathbb{R}^p} \|(L^{\top})^{\dagger} \partial_{\rho} f + LZ\eta\|_2^2 = \operatorname{argmin}_{\eta \in \mathbb{R}^p} \|(L^{\top})^{\dagger} \partial_{\rho} f + Y\eta\|_2^2, \quad \text{where } Y = LZ,$$

for a matrix L representing the discretization of the continuous operator \mathbf{L} for different metric spaces as discussed in Section 2. We regard (3.2) as a unified framework since changing the metric space for the natural gradient only requires changing L while the other components remain fixed.

Note that one can compute the standard gradient $\partial_\theta f = \partial_\theta \rho^\top \partial_\rho f = Z^\top \partial_\rho f$ by chain rule. From (3.2), we can also obtain the common formulation for the natural gradient descent as

$$(3.3) \quad \begin{aligned} \eta_L^{nat} &= -(Z^\top L^\top LZ)^{-1} (Z^\top L^\top (L^\top)^\dagger \partial_\rho f) = -(Y^\top Y)^{-1} (Z^\top \partial_\rho f) \\ &= -(Y^\top Y)^{-1} \partial_\theta f = -G_L^{-1} \partial_\theta f, \end{aligned}$$

where $G_L = Y^\top Y$ is the corresponding information matrix defined in (2.5).

Remark 3.1. The unified framework (3.2) is general and applies to cases beyond natural gradients discussed in Section 2. For ρ in a metric space (\mathcal{M}, g) with a corresponding tangent space $T_\rho \mathcal{M}$, we have

$$\langle \zeta_1, \zeta_2 \rangle_{g(\rho)} \approx \vec{\zeta}_1^\top A_\rho^g \vec{\zeta}_2, \quad \forall \zeta_1, \zeta_2 \in T_\rho \mathcal{M},$$

where $\vec{\zeta}_1, \vec{\zeta}_2$ denote the discretized ζ_1, ζ_2 . A proper discretization that preserves the metric structure should yield a symmetric positive definite matrix A_ρ^g that admits decomposition $A_\rho^g = L^\top L$. As a result, the discretization of (2.4) turns into the same formula as (3.2):

$$\begin{aligned} \eta_L^{nat} &= -(Z^\top A_\rho^g Z)^{-1} (Z^\top \partial_\rho f) = -(Z^\top L^\top LZ)^{-1} (Z^\top L^\top (L^\top)^\dagger \partial_\rho f) \\ &= \operatorname{argmin}_{\eta \in \mathbb{R}^p} \|(L^\top)^\dagger \partial_\rho f + Y\eta\|_2^2, \quad \text{where } Y = LZ. \end{aligned}$$

The concrete form of L will depend on the specific metric space (\mathcal{M}, g) .

Next, we will first assume that L is given and discuss how to compute η_L^{nat} provided whether the Jacobian Z is available or not; see Subsection 3.2 and Subsection 3.3. Later in Subsection 3.4, we will comment on obtaining the matrix L based on the natural gradient examples in Section 2.

3.2. Z available. When Z is available, there are two main methods to compute η_L^{nat} .

One may follow (3.3) by first constructing the information matrix $G_L = Y^\top Y$ and then computing its inverse. This is a reasonable method when the number of parameters, i.e., p , is small, and G_L is invertible. However, if G_L is singular or has bad conditioning, it is *more advantageous* to compute η_L^{nat} following (3.2). Note that the condition number of G_L can be nearly the square of the condition number of L , making it more likely to suffer from numerical instabilities.

The second and also our recommended approach is to solve the least-squares problem (3.2). We may utilize the QR factorization to do so [12]. Assume that $Y = LZ$ has full column rank. Let $Y = QR$ where Q has orthonormal columns and R is an upper triangular square matrix. Thus,

$$\eta_L^{nat} = -Y^\dagger (L^\top)^\dagger \partial_\rho f = -R^{-1} Q^\top (L^\top)^\dagger \partial_\rho f.$$

The additional computational cost of evaluating η_L^{nat} after the QR decomposition is the backward substitution to evaluate R^{-1} instead of inverting R directly.

If the given model $\rho(\theta)$ allows us to write down how ρ depends on θ analytically, then the Jacobian $\partial_\theta \rho$ is readily available. In such cases, we can directly solve (3.2) using the QR decomposition to obtain the natural gradient descents; see Subsection 4.1 for a Gaussian mixture example.

3.3. Z unavailable. Often, the model $\rho(\theta)$ is not available analytically, but the relationship between ρ and θ is given implicitly via solutions of a system, e.g., a PDE constraint,

$$(3.4) \quad h(\rho, \theta) = \mathbf{0},$$

for some smooth $h : \mathbb{R}^k \times \mathbb{R}^p \rightarrow \mathbb{R}^k$ such that $\det(\partial_\rho h) \neq 0$. In such cases, the Jacobian $Z = \partial_\theta \rho$ in (3.1) is not readily available and has to be computed or implicitly evaluated.

3.3.1. The implicit function theorem and adjoint-state method. Based on the first-order variation of (3.4), the most direct option to proceed is to apply the implicit function theorem

$$(3.5) \quad \partial_\rho h \partial_\theta \rho = \partial_\rho h Z = -\partial_\theta h.$$

The above equation consists of p linear systems in k variables. If $\partial_\rho h$ has a simple format, or the size of θ is not too large, it could still be computationally feasible to first obtain $Z = \partial_\theta \rho$ by solving (3.5), and then follow strategies in Subsection 3.2 to compute the natural gradient descent.

However, if p is large, a more efficient option is to use methods based on the so-called adjoint-state method [31]. Note that Z is the rate of change of the *full state* ρ with respect to θ . Thus, if we only need the rate of change of ρ *along a specific vector* $\xi \in \mathbb{R}^k$, we do not need the whole Z ; instead, we need $\xi^\top Z$ which can be calculated by solving only one linear system for each ξ .

Indeed, for a given $\xi \in \mathbb{R}^k$, let us consider the *adjoint equation*

$$(3.6) \quad \lambda_\xi^\top \partial_\rho h = \xi^\top \iff (\partial_\rho h)^\top \lambda_\xi = \xi.$$

Combining (3.5) and (3.6), we obtain that

$$(3.7) \quad Z^\top \xi = Z^\top (\partial_\rho h)^\top \lambda_\xi = -\partial_\theta h^\top \lambda_\xi.$$

The vector λ_ξ in (3.6) is called the *adjoint variable* corresponding to the given vector ξ .

Here is an important example where we do not need the full Z . If we choose $\xi = \partial_\rho f \in \mathbb{R}^k$, then (3.7) gives the standard gradient

$$(3.8) \quad D_\theta f(\rho(\theta)) = \partial_\theta \rho^\top \partial_\rho f = Z^\top \partial_\rho f = -\partial_\theta h^\top \lambda_\xi,$$

where λ_ξ is the solution to (3.6) with $\xi = \partial_\rho f \in \mathbb{R}^k$. This is a widely used method to efficiently evaluate the gradient of a large-scale optimization in solving PDE-constrained optimization problems originated from optimal control and computational inverse problems [31].

Next, we will explain in detail how to harness the power of the adjoint-state method to evaluate the general *natural* gradient descent directions through iterative methods.

3.3.2. Krylov subspace methods. Given an arbitrary vector $\eta \in \mathbb{R}^p$, we may evaluate

$$(3.9) \quad G_L \eta = Z^\top L^\top L Z \eta$$

through the adjoint-state method even if we cannot access the information matrix G_L since the Jacobian Z is unavailable directly. Let $\hat{\rho} \in \mathbb{R}^k$ be an arbitrary vector, and consider the following constrained optimization problem [26]

$$(3.10) \quad \min_{\rho} J(\rho(\theta)) = \rho^\top \hat{\rho}, \quad \text{s.t. } h(\rho(\theta), \theta) = \mathbf{0}.$$

Note that this objective function $J(\rho(\theta))$ in (3.10) is different from the main objective function (1.1) but with the same constraint (3.4). A direct calculation reveals that the gradient of $J(\rho(\theta))$ with respect to the parameter θ is $Z^\top \hat{\rho}$. Therefore, if we set $\hat{\rho} = L^\top L Z \eta$, the gradient

$$D_\theta J(\rho(\theta)) = Z^\top \hat{\rho} = Z^\top L^\top L Z \eta = G_L \eta,$$

which is exactly what we aim to compute in (3.9).

From the constraint $h(\rho(\theta), \theta) = \mathbf{0}$ and its first-order variation (3.5), we have

$$\partial_\rho h Z \eta + \partial_\theta h \eta = \mathbf{0}.$$

Thus, $Z \eta$ can be obtained as the solution to a linear system with respect to γ :

$$(3.11) \quad \partial_\rho h \gamma = -\partial_\theta h \eta.$$

Based on the adjoint-state method introduced in Section 3.3.1, we can compute the gradient as

$$D_\theta J(\rho(\theta)) = -\partial_\theta h^\top \lambda,$$

where λ satisfies the adjoint equation below with a given γ that solves (3.11),

$$(3.12) \quad \partial_\rho g^\top \lambda = \partial_\rho J = \hat{\rho} = L^\top L Z \eta = L^\top L \gamma.$$

To sum up, with a fixed θ and the corresponding $\rho(\theta)$, we have an efficient way to evaluate the linear action $G_L \eta$ for any given η by the following three steps.

- (1) Given η , solve the linear system (3.11) to obtain γ .
 - (2) Given γ and $L^\top L$, solve the linear system (3.12) to obtain λ ,
 - (3) Evaluate $-\partial_\theta h^\top \lambda$, which is equal to the linear action $G_L \eta$.
- Given the linear action G_L , we need to solve the linear system

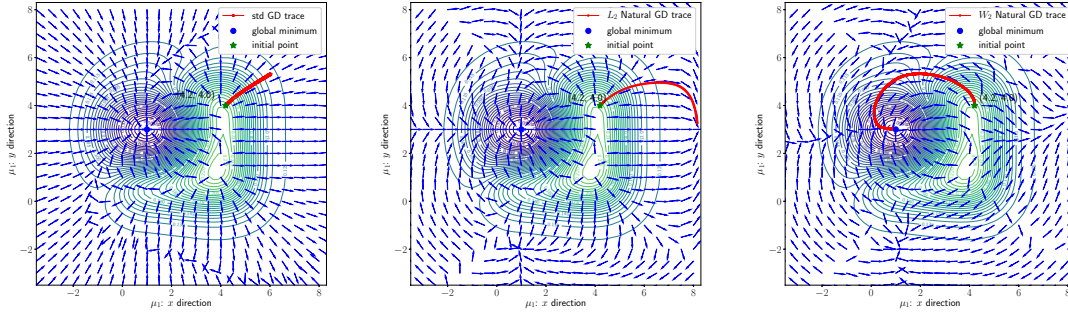
$$G_L \eta_L^{nat} = -D_\theta f(\rho(\theta))$$

to find the natural gradient descent direction η_L^{nat} . As seen in (3.8), we can obtain the right-hand side $-D_\theta f(\rho(\theta))$ through the adjoint-state method. One may then solve for η_L^{nat} through iterative linear solvers based on the Krylov subspace methods [33]. The conjugate gradient method is particularly preferable since this is a symmetric positive semi-definite linear system.

3.4. Natural gradient examples. In Subsection 3.2 and Subsection 3.3, we have discussed how to compute the natural gradient descent direction η_L^{nat} given Z is easily available or not. The strategies therein require the matrix L , which depends on the particular metric space for the natural gradient. In this subsection, we specify the form of L based on cases discussed in Section 2.

The L^2 case in Subsection 2.1 corresponds to $L = I$, the $k \times k$ identity matrix, while the Fisher–Rao–Hellinger natural gradient discussed in Subsection 2.4 corresponds to $L = \text{diag} \left(\frac{1}{\sqrt{\rho}} \right) \in \mathbb{R}^{k \times k}$. For the H^s natural gradient discussed in Subsection 2.2, L corresponds to proper discretization of \mathbf{D}^s (for $s > 0$) and $((\mathbf{D}^{-s})^*)^\dagger$ (for $s < 0$). Similarly, for the \dot{H}^s natural gradient discussed in Subsection 2.3, L should correspond to proper discretization of $\tilde{\mathbf{D}}^s$ (for $s > 0$) and $((\tilde{\mathbf{D}}^{-s})^*)^\dagger$ (for $s < 0$). Based on the unweighted reformulation (2.27), computing the W_2 natural gradient descend direction requires the discretization of $\mathbf{L} = \mathbf{B}^\dagger$. We can first discretize the differential operator \mathbf{B} , denoted as B , and then compute $L = B^\dagger$, which can be used no matter the Jacobian $Z = \partial_\theta \rho$ is explicitly given or implicitly provided through the constraint (3.4).

4. Numerical results. In this section, we present two optimization examples to illustrate the effectiveness of our computational strategies for natural gradient descent methods. We first present the parameter reconstruction of a Gaussian mixture model in Subsection 4.1 where the Jacobian $\partial_\theta \rho$ is explicitly given. We show that different (natural) gradient descent methods converge to different stationary points of a nonconvex objective function. We then present a large-scale waveform inversion problem in Subsection 4.2, which is a PDE-constrained optimization problem where the Jacobian $\partial_\theta \rho$ is not explicitly given. Using our computational strategy proposed in Subsection 3.3, we can efficiently implement the natural gradient descent method based on a general metric space. Our second example illustrates that different (natural) gradient descent methods have various convergence rates. Both phenomena are interesting as they indicate that one may achieve global convergence or faster convergence by choosing a proper metric space (\mathcal{M}, g) that fits the problem.



(a) Standard gradient descent (b) L^2 natural gradient descent (c) W_2 natural gradient descent

Figure 1: Gaussian mixture model setting one: level sets, vector fields and convergent paths for inverting μ_1 starting from $(4.2, 4)$ using the standard, L^2 and W_2 natural gradient descents.

4.1. Gaussian mixture model. Consider the Gaussian mixture model, which assumes that all the data points are generated from a mixture of a finite number of normal distributions with unknown parameters. Consider a probability density function $\rho(x; \theta) : \mathbb{R}^d \mapsto \mathbb{R}^+$ where

$$\rho(x; \theta) = w_1 \mathcal{N}(x; \mu_1, \Sigma_1) + \dots + w_i \mathcal{N}(x; \mu_i, \Sigma_i) + \dots + w_k \mathcal{N}(x; \mu_k, \Sigma_k).$$

The i -th Gaussian, denoted as $\mathcal{N}(x; \mu_i, \Sigma_i)$ with the mean vector $\mu_i \in \mathbb{R}^d$ and the covariance matrix $\Sigma_i \in \mathbb{R}^{d \times d}$, has a weight factor $w_i \geq 0$. Note that $\sum_i w_i = 1$. Here, θ could represent parameters such as $\{w_i\}$, $\{\mu_i\}$ and $\{\Sigma_i\}$. We formulate the inverse problem of finding the parameters as a data-fitting problem by minimizing the least-squares loss $f(\rho(\theta))$ on a compact domain Ω where the objective function follows (2.28). Here, ρ^* is the observed reference density function. Note that the dependence between the state variable ρ and the parameter θ is explicit here. Thus, we can compute the Jacobian $\partial_\theta \rho$ analytically, and the calculation for the natural gradient descent directions will follow Subsection 3.2.

4.1.1. Setting one. Let $d = 2$, $\rho^*(x) = 0.3\mathcal{N}(x; (1, 3), I) + 0.7\mathcal{N}(x; (3, 2), I)$ and θ be either μ_1 or μ_2 while the other parameters in this two-mixture model are fixed to be correct. This setting degenerates to the problem of comparing two Gaussians, but there are some interesting behaviors from different (natural) gradient descent methods given a truncated domain $\Omega = [0, 5]^2$.

In Figure 1, we present results reconstructing μ_1 using the standard, the L^2 and W_2 natural gradient descents. The vector fields (colored in blue) in all subplots disclose the drastic differences among the three different descent methods, leading to their qualitatively different convergence behavior. Both the standard and L^2 natural gradient descent methods converge to local minimizers while the W_2 natural gradient descent method converges to the global minimum $(1, 3)$.

We aim to gain better understandings regarding their different convergence behaviors. Given a fixed l -th iterate, all three methods proceed to find the $(l + 1)$ -th iterate, but based on different “principles” in terms of the proximal operators (1.3) and (1.2). Here, we use $\theta_{\text{std}}^{l+1}$, $\theta_{W_2}^{l+1}$ and $\theta_{L^2}^{l+1}$ to

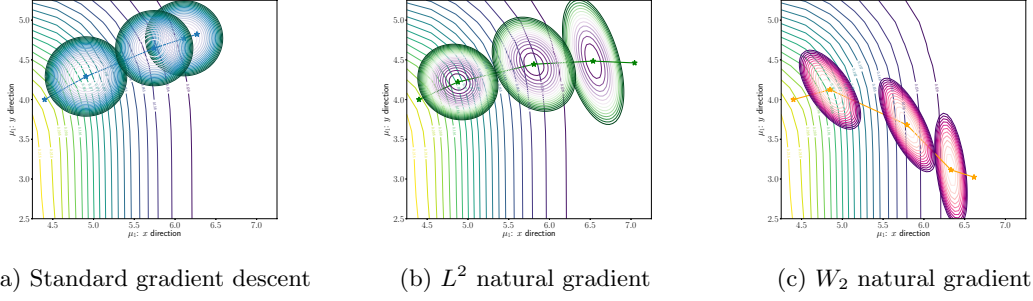


Figure 2: The local quadratic models of the three gradient methods in the first several iterations.

denote the next iterates based on these three methods, respectively. We then have

$$\begin{aligned}\theta_{\text{std}}^{l+1} &= \underset{\theta}{\operatorname{argmin}} \left\{ f(\rho(\theta)) + \frac{\|\theta - \theta^l\|^2}{2\tau} \right\} \approx \theta^l + \underset{h}{\operatorname{argmin}} \left\{ \nabla_{\theta} f^{\top} h + \frac{1}{2\tau} h^{\top} h \right\}, \\ \theta_{L^2}^{l+1} &= \underset{\theta}{\operatorname{argmin}} \left\{ f(\rho(\theta)) + \frac{\|\rho(\theta) - \rho(\theta^l)\|_2^2}{2\tau} \right\} \approx \theta^l + \underset{h}{\operatorname{argmin}} \left\{ \nabla_{\theta} f^{\top} h + \frac{1}{2\tau} h^{\top} \partial_{\theta} \rho^{\top} \partial_{\theta} \rho h \right\}, \\ \theta_{W_2}^{l+1} &= \underset{\theta}{\operatorname{argmin}} \left\{ f(\rho(\theta)) + \frac{W_2^2(\rho(\theta), \rho(\theta^l))}{2\tau} \right\} \approx \theta^l + \underset{h}{\operatorname{argmin}} \left\{ \nabla_{\theta} f^{\top} h + \frac{1}{2\tau} h^{\top} (B^{\dagger} \partial_{\theta} \rho)^{\top} B^{\dagger} \partial_{\theta} \rho h \right\}.\end{aligned}$$

The above equations show that, locally, the three (natural) gradient descent methods solve three different quadratic problems given the same step size τ , which explains their different convergence paths given the same initial point. In [Figure 2](#), we illustrate the level set of each quadratic problem for which the minimum is selected as the next iterate. The level sets of the objective function $f(\rho(\theta))$ are shown in the background. The differences in the local geometry may help explain why different (natural) gradient descent methods qualitatively converge to various stationary points. Our observation here is aligned with the example shown in [\[9, Fig. 3\]](#).

4.1.2. Setting two. We consider reference $\rho^*(x) = 0.3\mathcal{N}(x; (1, 3), 0.6I) + 0.7\mathcal{N}(x; (3, 2), 0.6I)$ and the domain $\Omega = [-2.75, 7.25]^2$. We fix μ_2 and the weights to be incorrect and invert $\theta = \mu_1$. That is, $\rho(x; \theta) = 0.2\mathcal{N}(x; \theta, 0.6I) + 0.8\mathcal{N}(x; (4, 3), 0.6I)$. [Figure 3](#) shows the convergence paths of the L^2 and the W_2 natural gradient descent methods under two different initial guesses: $(5, 3)$ and $(4.5, 3.5)$. The W_2 natural gradient method converges the global minimum under both initial points while the L^2 natural gradient method converges to two different local minima.

4.1.3. Setting three. Consider the same reference model as in setting two, and the domain $\Omega = [-5.5, 9.5]^2$. The parameterized model $\rho(x; \theta) = w\mathcal{N}(x; (\mu_{11}, 2), 0.6I) + (1-w)\mathcal{N}(x; (2.5, 1.5), 0.6I)$. We aim to find the weight w and the first element of vector μ_1 , denoted as μ_{11} . [Figure 4](#) shows the convergence paths of the standard, the L^2 , the W_2 and the Fisher–Rao natural gradient descent methods under the same initial guess. The standard gradient descent and the L^2 natural gradient descent converge to the same stationary point but with different trajectories while the latter two methods both converge to the global minimizer with very similar convergence paths.

4.2. Full waveform inversion. We present a full waveform inversion (FWI) example where the Jacobian is not explicitly given. As a PDE-constrained optimization, the dependence between the data and the parameter is implicitly given through the scalar wave equation

$$(4.1) \quad m(x)u_{tt}(x, t) + \triangle u(x, t) = s(x, t),$$

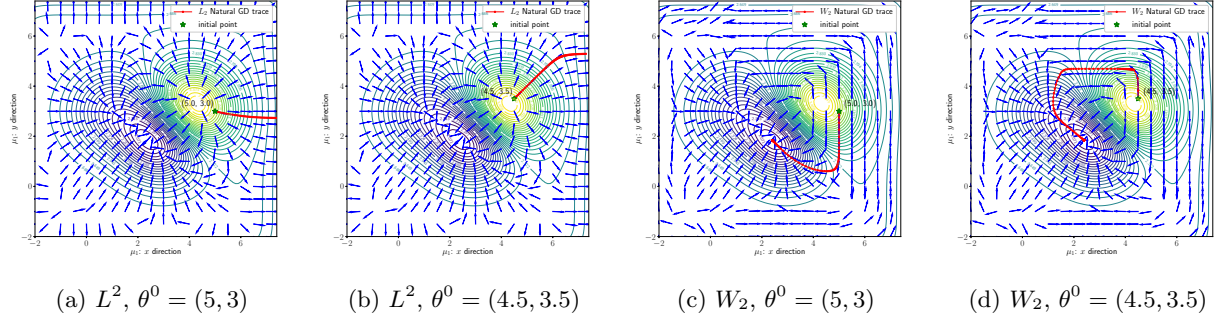


Figure 3: Gaussian Mixture Setting Two: level sets, vector fields and convergent paths using the L^2 and W_2 natural gradient descent methods to invert μ_1 . Here, (a) and (c) start from initial guess $(5, 3)$ while (b) and (d) start from $(4.5, 3.5)$. Other parameters are fixed to be incorrect.

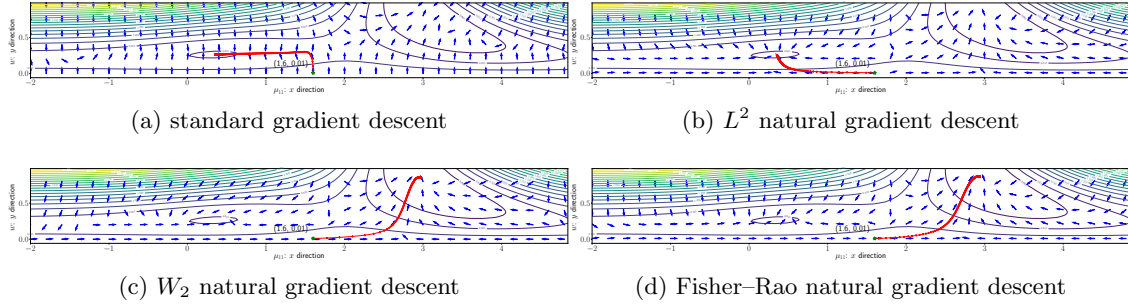


Figure 4: Gaussian Mixture Setting Three: level sets, vector fields and convergent paths using the four (natural) gradient methods for inverting the first component of μ_1 and the weight w . Other parameters are fixed to be either the correct or incorrect values.

where $s(x, t)$ is the source term and (4.1) is equipped with the initial condition $u(x, 0) = u_t(x, 0) = 0$ and an absorbing boundary condition to mimic the unbounded domain.

After discretization, the unknown function $m(x)$ becomes a finite number of unknowns, which we denote by θ for consistency. Unlike the Gaussian mixture model, the size of θ in this example is large as $p = 36720$. We obtain the observed data $\rho_r = u(x_r, t)$ at a sequence of receivers $\{x_r\}$, for $r = 1, \dots, n_r$. The least-squares objective function is

$$(4.2) \quad f(\rho(\theta)) = \frac{1}{2} \sum_{i=1}^{n_s} \sum_{r=1}^{n_r} \|\rho_{i,r}^* - \rho_{i,r}(\theta)\|_2^2,$$

where ρ^* is the observed reference data, and i is the source term index to consider inversions with multiple sources $\{s_i(x, t)\}$ as the right-hand side in (4.1). In our test, $n_s = 21$ and $n_r = 306$.

The true parameter is presented in Figure 5a. We remark that minimizing (4.2) with the constraint (4.1) is a highly nonconvex problem [38]. We avoid dealing with the nonconvexity by choosing a good initial guess as shown in Figure 5b. One may also choose other objective functions such as the Wasserstein metric to improve the optimization landscape [11]. We follow Subsection 3.3 to carry out the implementation for various natural gradient descent methods since the Jacobian $\partial_\theta \rho$ is not explicitly given, and the adjoint-state method has to be applied based on (4.1). The

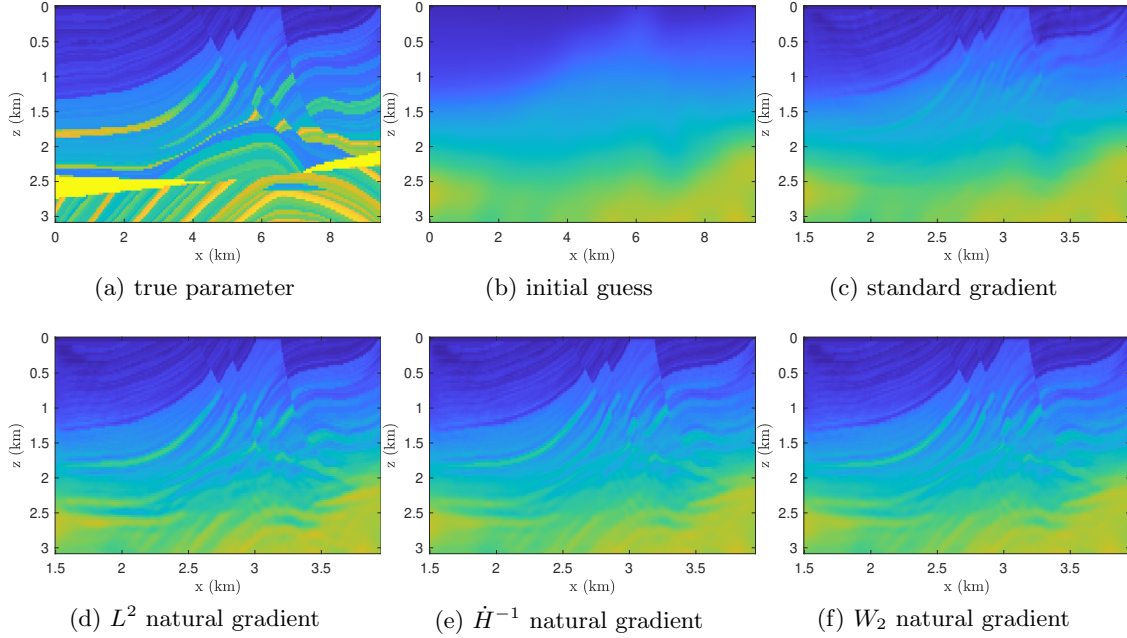


Figure 5: FWI example: (a) true parameter; (b) initial guess; (c)-(f) inversion after 100 iterations of the standard, L^2 natural, \dot{H}^{-1} natural and the W_2 natural gradient descent methods, respectively.

standard gradient descent (see Figure 5c) converges slowly compared to the natural gradient descent methods, while the L^2 natural gradient descent converges faster than the \dot{H}^{-1} and W_2 natural gradient descents as one can see in Figure 5e and Figure 5f in terms of image resolution. Note that wavefields are not naturally probability distributions. Thus, when we implement the W_2 natural gradient, we normalize the data to be probability densities following [10, 11]. As we have discussed in Remark 2.3, the W_2 and \dot{H}^{-1} natural gradients are closely related, which are also reflected in this numerical example as the reconstructions in Figure 5e and Figure 5f are very similar. All the tests shown in Figure 5 directly demonstrate that the natural gradient descent is typically faster than the standard gradient descent, and more importantly, the choice of the metric space (\mathcal{M}, g) for the natural gradient descent in (2.2) also has a direct impact on the convergence rate.

5. Conclusions. We present a unified framework to apply the natural gradient descent method based on a general metric space (\mathcal{M}, g) to solve large-scale optimization problems. The first main contribution of this work is to reformulate various natural gradients as standard L^2 -based least-squares problems on the continuous level. After discretization, the natural gradient descent directions can be efficiently computed through mature techniques from numerical linear algebra. The second main contribution is proposing computational strategies targeting two common scenarios in optimization tasks from computational inverse problems: whether the continuous dependence between the observed state variable and the parameter is explicitly given by the model or implicitly provided through the optimization constraints. The latter is commonly seen in large-scale PDE-constrained optimization problems. We provide each case with a numerical example using the proposed method. Our third contribution is the numerical investigation of the convergence behaviors from the standard gradient descent and the natural gradient descent methods based upon different metric spaces. Empirical results indicate that the choice of the metric space in a natural gradient descent not only can change the rate of convergence but also influence the stationary point

where the iterates converge, given a nonconvex optimization landscape. The numerical results shed light on a promising future research direction: how to choose the metric space properly such that the iterates can converge faster without increasing the computational cost or are led to a particular target stationary point such as the global minimum. These are interesting problems related to optimal design, optimal control, and computational inverse problems.

Acknowledgments. L. Nurbekyan was partially supported by AFOSR MURI FA 9550 18-1-0502 grant. W. Lei was partially supported by the 2021 Summer Undergraduate Research Experience (SURE) at the Department of Mathematics, Courant Institute of Mathematical Sciences, New York University. Y. Yang was partially supported by the National Science Foundation under Award Number DMS-1913129. This work was done in part while Y. Yang was visiting the Simons Institute for the Theory of Computing in Fall 2021. Y. Yang also acknowledges supports from Dr. Max Rössler, the Walter Haefner Foundation and the ETH Zürich Foundation.

REFERENCES

- [1] S.-I. AMARI, *Differential-geometrical methods in statistics*, vol. 28, Springer Science & Business Media, 1985.
- [2] S.-I. AMARI, *Natural gradient works efficiently in learning*, Neural computation, 10 (1998), pp. 251–276.
- [3] S.-I. AMARI AND A. CICHOCKI, *Adaptive blind signal processing-neural network approaches*, Proceedings of the IEEE, 86 (1998), pp. 2026–2048.
- [4] S.-I. AMARI AND S. C. DOUGLAS, *Why natural gradient?*, in Proceedings of the 1998 IEEE International Conference on Acoustics, Speech and Signal Processing, ICASSP’98 (Cat. No. 98CH36181), vol. 2, IEEE, 1998, pp. 1213–1216.
- [5] L. AMBROSIO, E. BRUÉ, AND D. SEMOLA, *Lectures on optimal transport*, Springer, 2021.
- [6] L. AMBROSIO, N. GIGLI, AND G. SAVARÉ, *Gradient flows in metric spaces and in the space of probability measures*, Lectures in Mathematics ETH Zürich, Birkhäuser Verlag, Basel, second ed., 2008.
- [7] M. ARBEL, A. GRETTON, W. LI, AND G. MONTUFAR, *Kernelized Wasserstein natural gradient*, in International Conference on Learning Representations, 2020.
- [8] L. BOTTOU, F. E. CURTIS, AND J. NOCEDAL, *Optimization methods for large-scale machine learning*, SIAM Review, 60 (2018), pp. 223–311.
- [9] Y. CHEN AND W. LI, *Optimal transport natural gradient for statistical manifolds with continuous sample space*, Information Geometry, 3 (2020), pp. 1–32.
- [10] B. ENGQUIST AND Y. YANG, *Seismic inversion and the data normalization for optimal transport*, Methods and Applications of Analysis, 26 (2019), pp. 133–148.
- [11] B. ENGQUIST AND Y. YANG, *Optimal transport based seismic inversion: Beyond cycle skipping*, Communications on Pure and Applied Mathematics, (2021).
- [12] G. H. GOLUB AND C. F. VAN LOAN, *Matrix computations. Johns Hopkins studies in the mathematical sciences*, Johns Hopkins University Press, Baltimore, MD, 1996.
- [13] N. D. HEAVNER, *Building rank-revealing factorizations with randomization*, PhD thesis, University of Colorado at Boulder, 2019.
- [14] M. E. KHAN AND H. RUE, *The Bayesian learning rule*, arXiv preprint arXiv:2107.04562, (2021).
- [15] W. LI, A. T. LIN, AND G. MONTÚFAR, *Affine natural proximal learning*, in Geometric Science of Information, F. Nielsen and F. Barbaresco, eds., Cham, 2019, Springer International Publishing, pp. 705–714.
- [16] W. LI, S. LIU, H. ZHA, AND H. ZHOU, *Parametric Fokker–Planck equation*, in Geometric Science of Information, F. Nielsen and F. Barbaresco, eds., Cham, 2019, Springer International Publishing, pp. 715–724.
- [17] W. LI AND G. MONTÚFAR, *Natural gradient via optimal transport*, Information Geometry, 1 (2018), pp. 181–214.
- [18] W. LI AND J. ZHAO, *Wasserstein information matrix*, 2020, <https://arxiv.org/abs/1910.11248>.
- [19] A. T. LIN, W. LI, S. OSHER, AND G. MONTÚFAR, *Wasserstein proximal of GANs*, in Geometric Science of Information, F. Nielsen and F. Barbaresco, eds., Cham, 2021, Springer International Publishing, pp. 524–533.
- [20] S. LISINI, D. MATTHES, AND G. SAVARÉ, *Cahn–Hilliard and thin film equations with nonlinear mobility as gradient flows in weighted-Wasserstein metrics*, Journal of Differential Equations, 253 (2012), pp. 814–850.
- [21] S. LIU, W. LI, H. ZHA, AND H. ZHOU, *Neural parametric Fokker–Planck equations*, arXiv preprint arXiv:2002.11309, (2020).
- [22] A. MALLASTO, T. D. HAIJE, AND A. FERAGEN, *A formalization of the natural gradient method for general similarity measures*, in Geometric Science of Information, F. Nielsen and F. Barbaresco, eds., Cham, 2019,

- Springer International Publishing, pp. 599–607.
- [23] J. MARTENS, *New insights and perspectives on the natural gradient method*, Journal of Machine Learning Research, 21 (2020), pp. 1–76.
 - [24] J. MARTENS AND R. GROSSE, *Optimizing neural networks with Kronecker-factored approximate curvature*, in International conference on machine learning, PMLR, 2015, pp. 2408–2417.
 - [25] J. MARTENS AND I. SUTSKEVER, *Training deep and recurrent networks with Hessian-free optimization*, in Neural networks: Tricks of the trade, Springer, 2012, pp. 479–535.
 - [26] L. MÉTIVIER, R. BROSSIER, J. VIRIEUX, AND S. OPERTO, *Full waveform inversion and the truncated Newton method*, SIAM Journal on Scientific Computing, 35 (2013), pp. B401–B437.
 - [27] Y. E. NESTEROV, *A method for solving the convex programming problem with convergence rate $O(1/k^2)$* , in Dokl. akad. nauk Sssr, vol. 269, 1983, pp. 543–547.
 - [28] J. NOCEDAL AND S. WRIGHT, *Numerical optimization*, Springer Science & Business Media, 2006.
 - [29] R. PASCANU AND Y. BENGIO, *Revisiting natural gradient for deep networks*, arXiv preprint arXiv:1301.3584, (2013).
 - [30] J. PETERS AND S. SCHAAL, *Natural actor-critic*, Neurocomputing, 71 (2008), pp. 1180–1190.
 - [31] R.-E. PLESSIX, *A review of the adjoint-state method for computing the gradient of a functional with geophysical applications*, Geophysical Journal International, 167 (2006), pp. 495–503.
 - [32] N. QIAN, *On the momentum term in gradient descent learning algorithms*, Neural networks, 12 (1999), pp. 145–151.
 - [33] Y. SAAD, *Iterative methods for sparse linear systems*, SIAM, 2003.
 - [34] N. N. SCHRAUDOLPH, *Fast curvature matrix-vector products for second-order gradient descent*, Neural Computation, 14 (2002), pp. 1723–1738.
 - [35] Z. SHEN, Z. WANG, A. RIBEIRO, AND H. HASSANI, *Sinkhorn natural gradient for generative models*, Advances in Neural Information Processing Systems, 33 (2020), pp. 1646–1656.
 - [36] P. THOMAS, B. C. SILVA, C. DANN, AND E. BRUNSKILL, *Energetic natural gradient descent*, in International Conference on Machine Learning, PMLR, 2016, pp. 2887–2895.
 - [37] C. VILLANI, *Topics in optimal transportation*, vol. 58 of Graduate Studies in Mathematics, American Mathematical Society, Providence, RI, 2003.
 - [38] J. VIRIEUX AND S. OPERTO, *An overview of full-waveform inversion in exploration geophysics*, Geophysics, 74 (2009), pp. WCC1–WCC26.
 - [39] H. H. YANG AND S.-I. AMARI, *Complexity issues in natural gradient descent method for training multilayer perceptrons*, Neural Computation, 10 (1998), pp. 2137–2157.
 - [40] Y. YANG, A. TOWNSEND, AND D. APPELÖ, *Anderson acceleration based on the \mathcal{H}^{-s} Sobolev norm for contractive and noncontractive fixed-point operators*, Journal of Computational and Applied Mathematics, 403 (2022), p. 113844.
 - [41] L. YING, *Natural gradient for combined loss using wavelets*, Journal of Scientific Computing, 86 (2021), pp. 1–10.